Karlsruher Institut für Technologie

Maximum shielding stress intensity factors in silica

K.G. Schell, C. Bucharsky, G. Rizzi, T. Fett

KIT SCIENTIFIC WORKING PAPERS 137

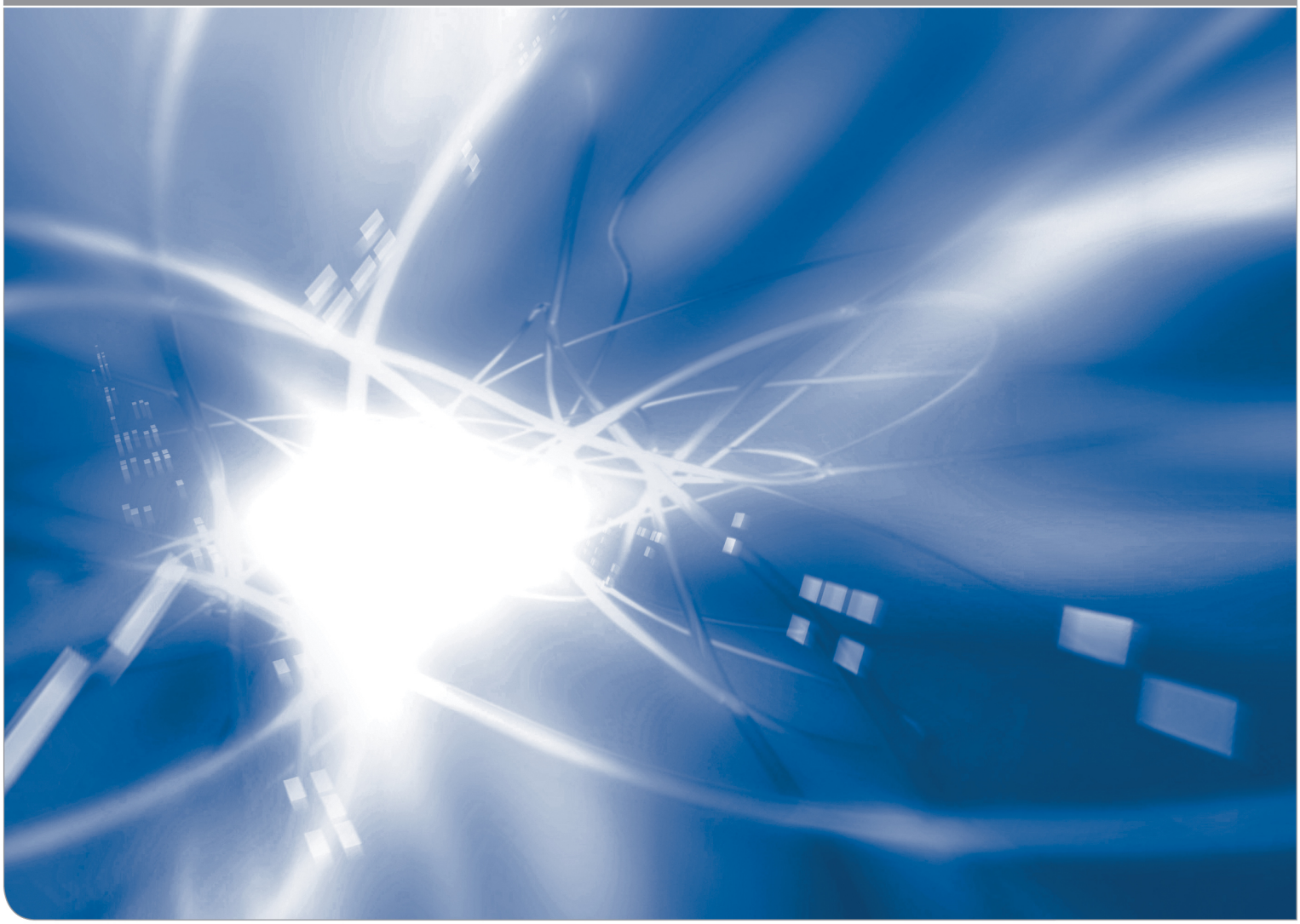

KIT – Universität des Landes Baden-Württemberg und nationales Forschungszentrum in der Helmholtz-Gemeinschaft

IAM Institute for Applied Materials

Impressum

Karlsruher Institut für Technologie (KIT)
www.kit.edu

2020

ISSN: 2194-1629

Abstract

When water penetrates into silica surfaces near a crack tip, it reacts with the SiO_2 network and generates hydroxyl ≡SiOH. Due to the hydroxyl generation, silica expands and gives rise for swelling stresses. The consequence is a fracture mechanics shielding stress intensity factor $K_{sh}<0$. The fracture mechanical treatment of swelling in the crack-tip region is significantly complicated by the occurrence of damage due to the production of hydroxyls.

A maximum possible shielding effect is obtained by using an asymmetry parameter $h=1$ in the crack wake ($\sigma_h<0$) and neglecting the tension region ahead the crack tip, where strong damage is present under hydrostatic tension ($\sigma_h>0$).

Contents

1. Introduction

The reaction of water and silica in the surface diffusion zone affects the fracture mechanics stress intensity factor K at the tips of cracks. At temperatures $T < 450°C$, the equilibrium constant of the water/silica-reaction

$$\equiv\text{Si-O-Si}\equiv + H_2O \leftrightarrow \equiv\text{SiOH+HOSi}\equiv \tag{1}$$

is given by

$$k_1 = \frac{S}{C}. \tag{2}$$

where, $S = [\equiv\text{SiOH}]$, is the concentration of the hydroxyl groups in the silica network and $C = [H_2O]$ the concentration of unreacted water.

According to Le Chatelier [1], the equation governing the equilibrium constant is

$$\frac{\partial \ln k_1}{\partial p} = -\frac{\Delta \overline{V}}{RT}. \tag{3}$$

where p is pressure, $\Delta \overline{V}$ is the reaction volume, R the universal gas constant, and T the temperature in °K.

In gases and liquids, the loading is always hydrostatic. In a solid the situation is more complicated, since the individual stress components σ_x, σ_y, σ_z are in general independent of each other and are not necessarily hydrostatic. Especially in uniaxial tension or compression, the hydrostatic stress deviates clearly from the tensile stress. In contrast to this, the stress state ahead of crack tips is more hydrostatic since the stress in the prospective plane and the stress normal on this plane are identical, $\sigma_x=\sigma_y$, and the stress σ_z is very close to the tip: $\sigma_z=\nu(\sigma_x+\sigma_y)$, ν=Poisson's ratio.

By replacing the hydrostatic pressure p by the hydrostatic stress σ_h in a solid

$$\sigma_h = \tfrac{1}{3}(\sigma_x + \sigma_y + \sigma_z) \tag{4}$$

we obtain with the hydroxyl concentration S_0 for $\sigma_h=0$

$$S = S_0 \exp\left(\frac{\sigma_h \Delta \overline{V}}{RT}\right) \quad , \quad \sigma_h = -p \tag{5}$$

Whereas in *uniaxial tension*, $\sigma=\sigma_y$, the ratio of the hydrostatic stress to the maximum stress is only

$$\sigma_h / \sigma_y = \tfrac{1}{3} \tag{6}$$

it holds along a prospective crack plane

$$\frac{\sigma_h}{\sigma_y} = \tfrac{2}{3}(1+\nu) \underset{\nu=0.17}{=} 0.78 \tag{7}$$

This value is much closer to the purely hydrostatic stress state described by $\sigma_h/\sigma_y=1$ and should therefore be applied to crack problems.
For a crack of depth *a*, the singular hydrostatic near-tip stresses are given as

$$\sigma_h = \tfrac{2}{3}(1+\nu)\frac{K}{\sqrt{2\pi r}}\cos(\varphi/2) \tag{8}$$

where *r* and φ are the polar coordinates with the origin at the crack tip, *K* is the stress intensity factor. Equations (5) and (8) imply that in the high crack-tip stress field nearly all water is present in form of hydroxyl *S*.
Subcritical crack growth tests in heavy water were carried out on DCDC specimens of silica by Lechenault et al. [2]. The water entrance into the fracture surfaces, formed by the passage of the crack exposed to deuterium oxide D_2O, was evaluated with a neutron reflection technique to measure the penetration of the deuterium oxide into the silica glass. The authors found a satisfactory fit to the reflection data by assuming that the water concentration was constant at the surface up to a distance of *L*, followed by an exponential decrease in concentration for distances greater than *L*.

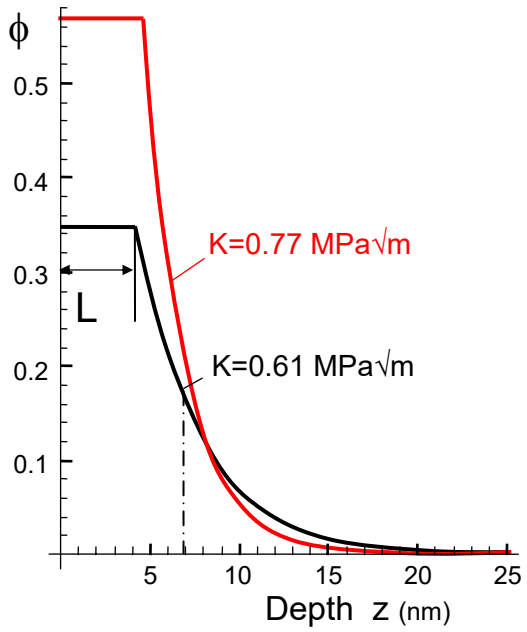

Fig. 1 Water profiles expressed by the neutron reflectivity ϕ measured by Lechenault et al. [2] on DCDC specimens fractured in heavy water.

Lechenault et al. [2] fitted their results by the expression

$$C_w / C_w(0) = \begin{cases} 1 & \text{for} \quad z \le L \\ \exp[-(z-L)/\eta] & \text{for} \quad z > L \end{cases} \tag{9}$$

and found the parameters L=4.3 nm, η=3.5 nm for a region of low crack rates ($v \approx 10^{-8}$ m/s) at K= 0.61 MPa·m$^{1/2}$ and L=4.6 nm, η=2.3 nm for higher crack rates ($v \approx 4\ 10^{-6}$ m/s) at K= 0.77 MPa·m$^{1/2}$. These water profiles are illustrated in Fig. 1. Their flat behaviour over an extended region calls for the application of the Dugdale- and the Irwin-model developed for linear-elastic perfectly plastic materials. Since in the crack-tip region the boundary conditions are not purely strain-controlled, as will be prescribed for the developments in Section 2, we will not yet make use of these models.

2 Hydroxyl damage under strain boundary conditions

The hydroxyl generation by the reaction eq.(1) causes damage since the originally intact silica ring structure is cracked by the water attack. One of the consequences of such damage is the reduction of Young's modulus E. In order to describe this E-decrease, we used in [3] the rather simple damage model proposed by Phany and Niyogi [4]. When E_D is the modulus in the damaged state and E_0 the value for undamaged silica, we could derive the relation [3]

$$\frac{E_D}{E_0} = (1 - \gamma S)^2 = (1 - S / S_{\max})^2 \tag{10}$$

with γ=5.3 [4.35, 6.25] (90%-CI in brackets). The hydroxyl concentration at which the Young's modulus disappears is $S_{\max}$ =1/γ= 0.188 [0.16, 0.23]. Under the condition that the damage is isotropic and Poisson's ratio ν remains sufficiently constant [5], the multiaxiality in damaged states remains unchanged. Then it holds for the individual normal stress components σ_i

$$\frac{\sigma_{i,D}}{\sigma_{i,0}} = \frac{\sigma_{h,D}}{\sigma_{h,appl}} \tag{11}$$

Let's consider a certain stress state with hydrostatic stress $\sigma_{h,appl}$ to a volume element of undamaged material with Young's modulus E_0 under strain boundary conditions. The strain- boundary conditions for Fig. 2 have to be understood in the following way: The volume element may contain molecular (unreacted) water in the unloaded state. The strain after load application is proportional to the loading, i.e.

$$\varepsilon_x, \varepsilon_y, \varepsilon_z \propto \frac{\sigma_{h,appl}}{E_0} \tag{12}$$

In the special case of $\sigma_x = \sigma_y = \sigma_z = \sigma_h$, the coefficient of proportionality is the "bulk module" $E/(3(1-2\nu))$. The strained volume is then fixed in this state and water-silica reaction is started.

The hydrostatic stress after hydroxyl generation and damaging, $\sigma_{h,D}$, decreases with decreasing Young's modulus:

$$\frac{\sigma_{h,D}}{\sigma_{h,appl}} = (1 - S / S_{\max})^2 \tag{13}$$

Consequently, the hydroxyl concentration as a function of the hydrostatic stress, eq.(5), can be written in the damaged state

$$S = S_0 \exp[\mu \sigma_{h,appl}(1 - S / S_{\max})^2], \qquad \mu = \frac{\Delta \overline{V}}{RT} \tag{14}$$

Equation (14) is an implicit equation since the unknown concentration S occurs on both sides. The solution can be found by numerical methods (e.g. by the subroutine *FindRoot* of Mathematica [6]).

Figure 2a shows the hydroxyl concentration as a function of $\sigma_{h,appl}$ and S_0. The effect of the coefficient μ is small for large $\mu \times \sigma_{h,appl}$. The hydroxyl generation by the reaction causes the reduction of Young's modulus from E_0 (undamaged state) to E_D (damaged state) according to eqs.(10, 11). The consequence is a reduction of the hydrostatic stress from $\sigma_{h,appl}$ to $\sigma_{h,D}$ in the damaged state (red arrow in Fig. 2b).

Figure 2b represents the hydrostatic stress under damage conditions as a function of the externally applied hydrostatic stress for several initial hydroxyl concentrations S_0. The maximum hydrostatic stress, asymptotically reached for $\sigma_{h.appl} \to \infty$, is according to eq.(5)

$$\sigma_{h,D,\max} = -\frac{1}{\mu} \mathrm{Log}\left[\frac{S_0}{S_{\max}}\right] \tag{15}$$

The true stresses $\sigma_{h,D}$ of Fig. 2b may be simplified by a bi-linear description as introduced by the dashed lines in Fig. 2c for $S_0 = 10^{-3}$. In this case the maximum possible stress in the damaged state is depending on the parameter μ, i.e. on temperature T: $\mu \sigma_{h,D,max} = 5.24$. In the sense of an upper limit solution, the stresses can be approximated as

$$\sigma_{h,D} = \begin{cases} \sigma_{h,appl} & \text{for} \quad \sigma_{h,appl} < \sigma_{h,D,\max} \\ \sigma_{h,D,\max} & \text{else} \end{cases} \tag{16}$$

The damage behaviour studied in this section is only addressed in order to show that the stresses at a crack tip must be limited as is the case for elastic-plastic materials.

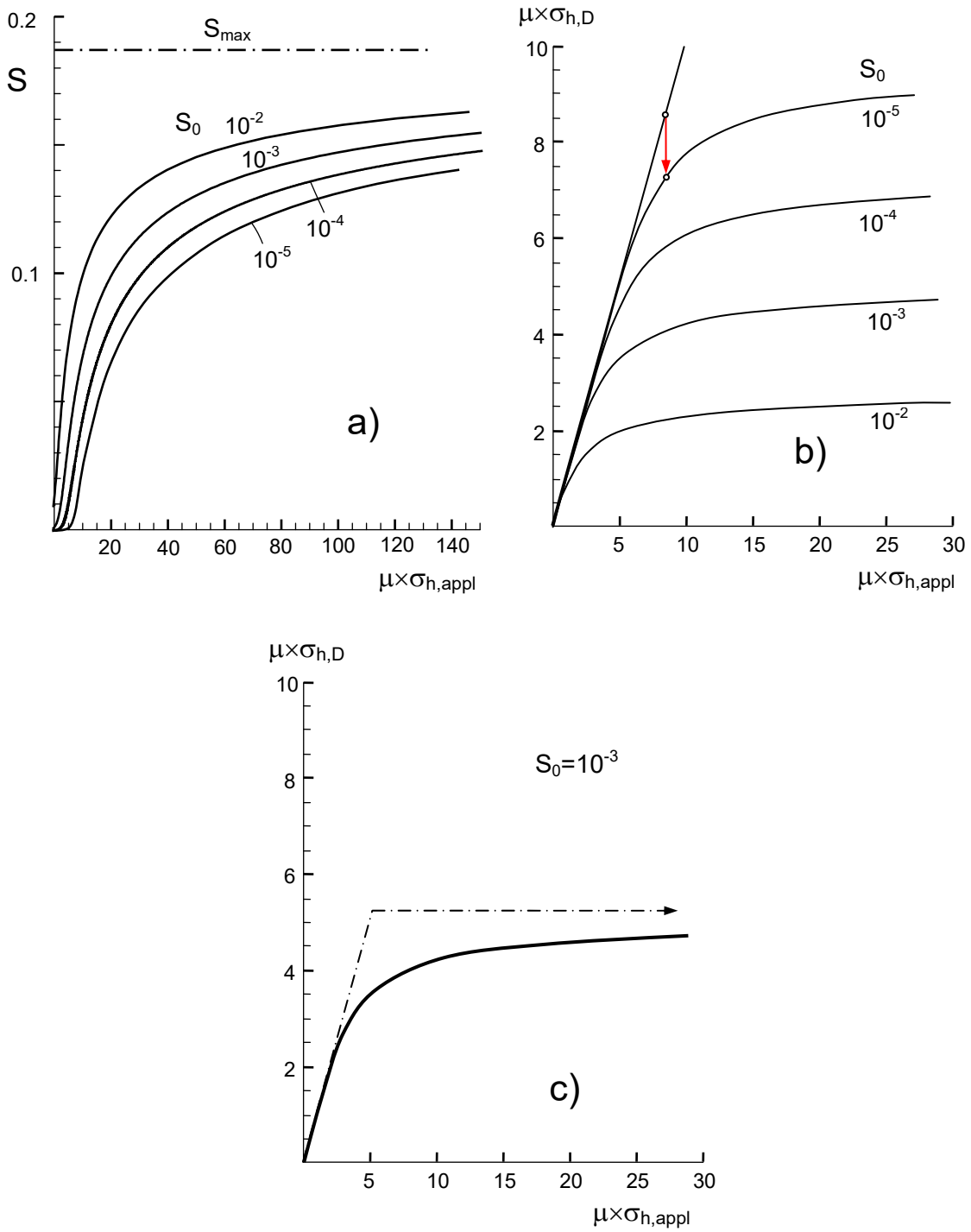

Fig. 2 a) Hydroxyl concentration vs. applied stress under condition of constant strains, b) hydrostatic stress in the damaged material $\sigma_{h,D}$ as a function of the applied hydrostatic stress $\sigma_{h,appl}$ and the hydroxyl concentration S_0 in the absence of stresses with the abbreviation μ defined by eq.(14), c) limit of hydrostatic stress and approximation by an upper bound description (dash-dotted straight lines).

3 Shielding stress intensity factor

For a zone of constant hydroxyl concentration and constant modulus over the height ω it holds:

$$K_{sh}\big|_{\varepsilon_v, E_D = const.} = -\psi \frac{\varepsilon_v E_D}{1-\nu}\sqrt{\omega} = -\psi \frac{\kappa S E_D}{1-\nu}\sqrt{\omega} \tag{17}$$

ν is Poisson's ratio of ν≅0.17.

The volume swelling strain ε_v can be computed from the hydroxyl concentration S

$$\varepsilon_v = \kappa S \tag{18}$$

with S in parts by mass and κ=0.97 [7].

Figure 3a shows the contour of a heart-shaped (black) and a semi-circular zone (red) for a crack starting to grow. In the range of φ<90°, the contours are hardly different. After a crack extension of Δa>5ω, Fig. 3b, the full shielding contribution is reached. The coefficient ψ was computed by McMeeking and Evans [8] with the result of ψ=0.22 for the heart-shaped zone contour, ψ=0.25 for a semi-circular profile, and ψ=0.37 if the contribution from material ahead of the tip is neglected, see Table 1 and Fig. 4. The value ψ=0.37 is regarded in [8] as an upper bound.

Damage Zone	Coefficient ψ	Case in Fig. 4	
Zone with heart-shaped end contour	0.22	(C)	
Zone with semi-circular end contour	0.25	(B)	
Semi-circular zone ahead the tip	-0.121		
Contributions behind the tip	0.37	(A)	Upper bound

Table 1 Coefficient ψ of eq.(17) for different shapes of swelling zones.

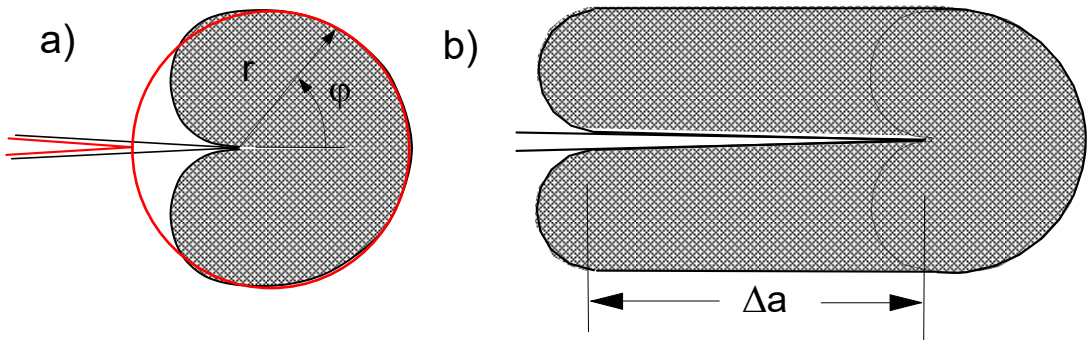

Fig. 3 a) Swelling zone with constant volume strain ε_v for an arrested crack, b) zone for a grown crack.

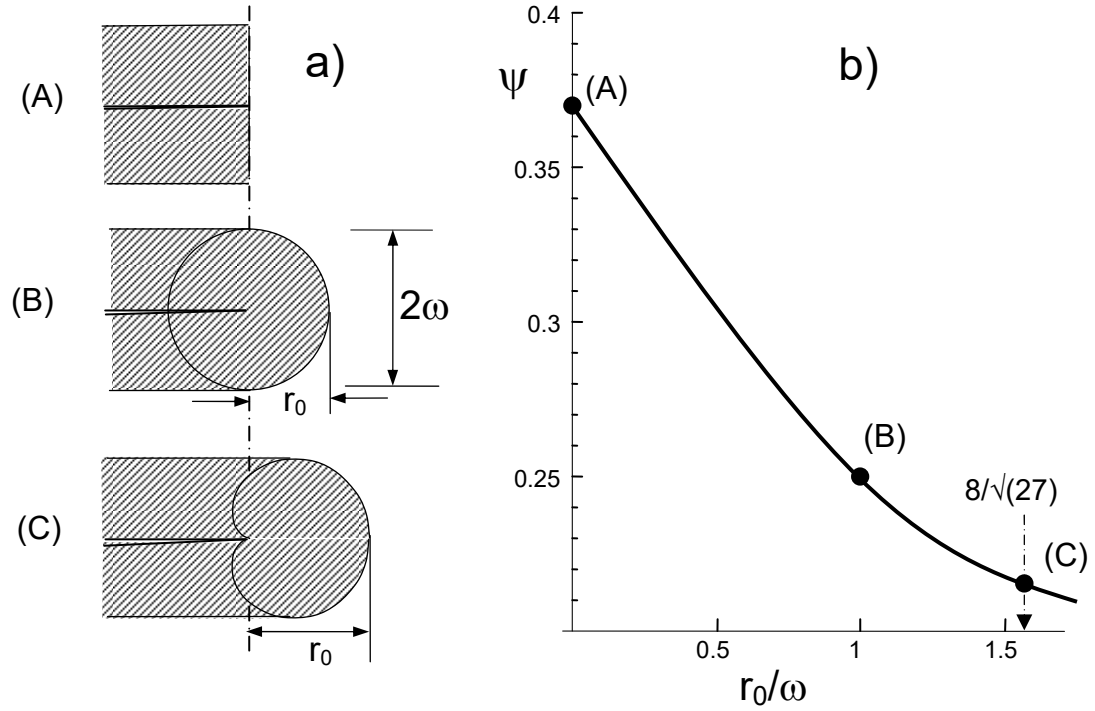

Fig. 4 Coefficient ψ of eq.(17), a) swelling zones with different shape at the zone end, b) results by McMeeking and Evans for constant volume swelling (circles) and interpolating curve.

4 Shielding stress intensity factor for asymmetric damage

In the case of disappearing total stress intensity factor at the crack tip, $K_{total} = K_{appl} + K_{tip} \leq 0$, all volume elements in the water-affected zone are under compression due to volume swelling by hydroxyl generation. In the previous considerations, we applied the model of pore-like defects. This model describes symmetrical material response under tension and compression loading. The Young's modulus in compression is not necessarily identical in tension and compression. This problem was handled by Lemaitre and Sermage [10] introducing non-symmetry of deformation in tension and compression. These authors included the case that the reduction of Young's modulus in compression is less strong than in tension by a non-symmetry coefficient or crack closure parameter $0 \leq h \leq 1$

$$E = \begin{cases} E_0(1-D) & \text{for} \quad \sigma \geq 0 \\ E_0(1-hD) & \text{for} \quad \sigma < 0 \end{cases} \tag{19}$$

with the "damage parameter" h and damage D by Lemaitre [9], defined as $D=1-E_D/E_0$. For most practical applications Lemaitre and Sermage suggest $h=0.2$ [10]. A possible reason for the differences in tension and compression is addressed in the Appendix.

The asymmetry gives reason to define an upper limit for the shielding stress intensity factor. The zone in front of the crack tip is under tension for a load of $K_{tip} > 0$, Fig. 5. The crack flanks, on the other hand, are stress-free with regard to the applied load and

are under pressure due to the swelling stresses. In this region the lower expression in (19) holds. As the limit approximation, the reduced modulus in the zone ahead of the tip is assumed to be free of any stress ($E_D \rightarrow 0$) and the crack-face region is assumed to exhibit the initial modulus, i.e. $h \rightarrow 0$. This approximation is also given by Eq. (17) by using the value $\boldsymbol{\psi = 0.37}$ according to McMeeking and Evans [8], see also Fig. 4.

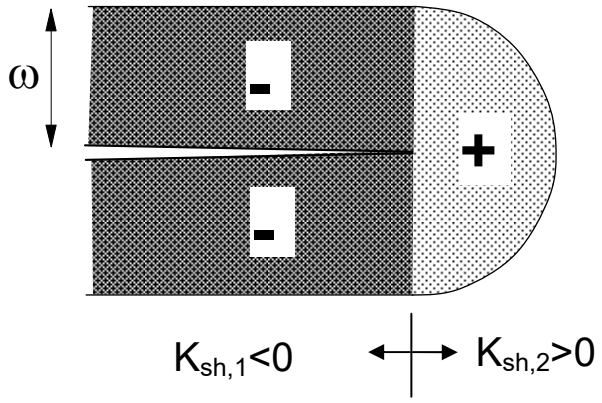

Fig. 5 Negative and positive contributions to the total shielding stress intensity factor.

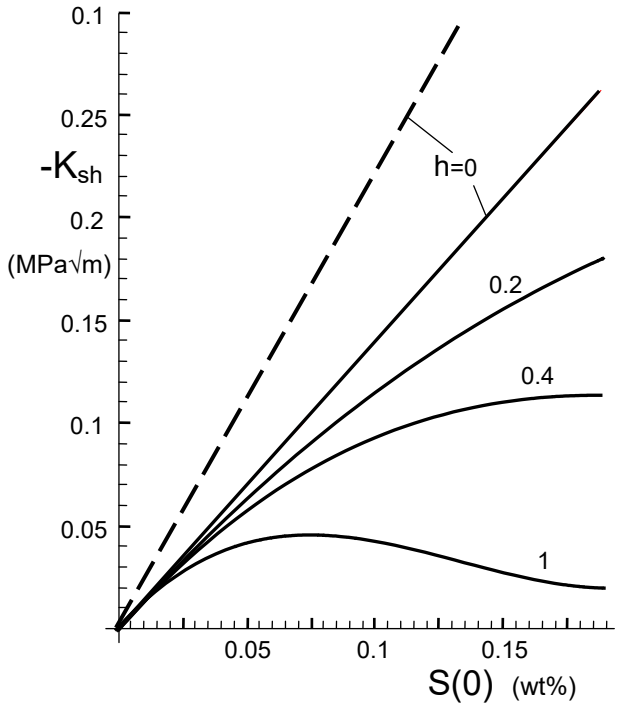

Fig. 6 Shielding stress intensity factors for an erfc-shaped hydroxyl distribution as a function of the surface concentration $S(0)$. Solid curves: from [11], dashed curve: eq.(17) with ψ=0.37.

Finally, Fig. 6 represents results from [11] for an erfc-shaped hydroxyl distribution with a surface value $S(0)$ and a parameter b of 4.95 nm (solid curves), according to:

$$S = S(0)\,\mathrm{erfc}\left[\frac{z}{2b}\right] \tag{20}$$

The dashed line in Fig. 6 shows the upper limit solution for the same *S*-distribution addressed before.

Outlook: Great similarities in the deformation behavior due to hydroxyl generation with elastic-plastic materials may give rise to the use of the well-known models by Irwin and Dugdale.

Appendix:

Mechanical interpretation of the limit case under compression

Figure 7a illustrates schematically the silica net structure attacked by a water molecule. A possible interpretation of the asymmetry coefficient h may be illustrated in the following way:

A SiO_2-ring of the silica network may be described by a spherical (nano)-void in a continuous material. This allows a fracture mechanics treatment by an FE-study. According to the finite crack-tip curvature for cracks, the radius of such a void has to be expected in the order of $\rho = 0.5$ nm [12], Fig. 7a.

Under a remote tensile load in z-direction, σ_∞, the red Si-O-bond may be cracked by reaction with molecular water (blue/red). In the tensile case the opened bond cannot transfer any significant tensile forces, Fig. 7b. Consequently, it is $h \rightarrow 1$ in eq.(19).

Due to the initially load-carrying fractured bond, the stress concentrations increase at the ends of the now tablet-shaped void as indicated by the red circles. Due to the exponential increase of the hydroxyl concentration with stress, newly reacting water molecules will predominantly react at these locations. Figure 8a illustrates the enlarged void when the water molecule might have reacted at the right side of Fig. 7b. Additional reactions will lead to micro-crack-like elongated defects perpendicular to the maximum principal stress.

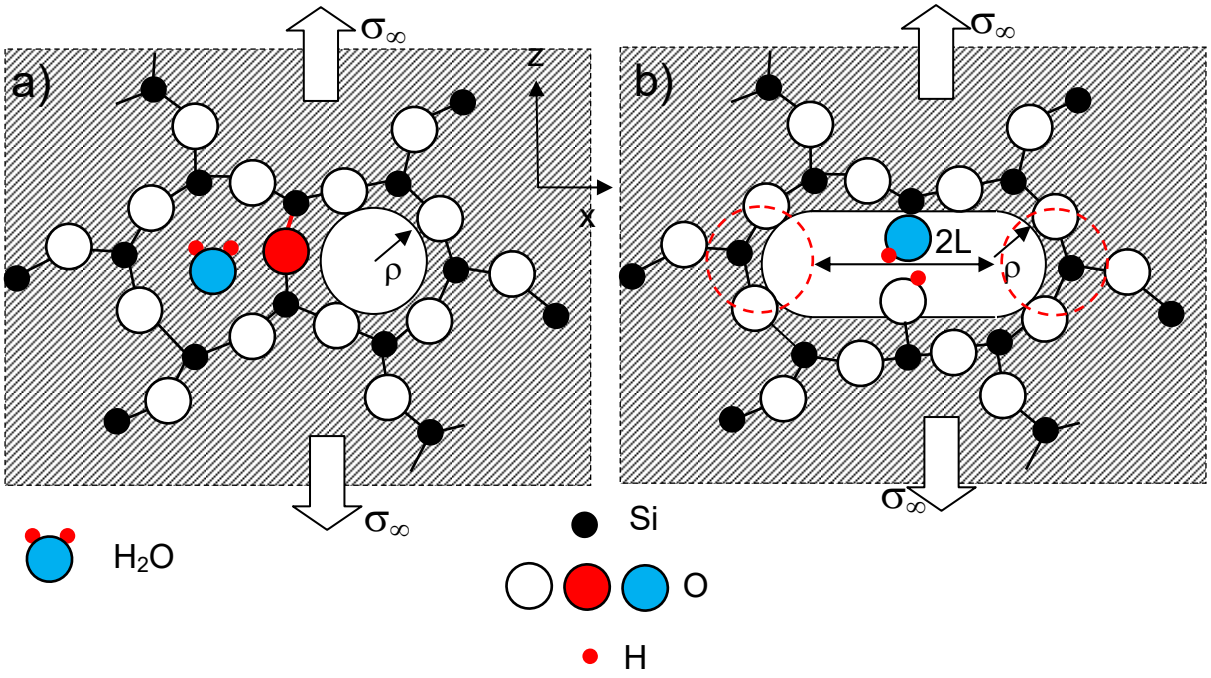

Fig. 7 a) Bond breaking under uni-axial tension by reaction with molecular water (attacked SiO_2-bond in red), b) limit case of an open bond represented by a disk-like notch of diameter $2(\rho+L)$, red circles: increased stress concentrations.

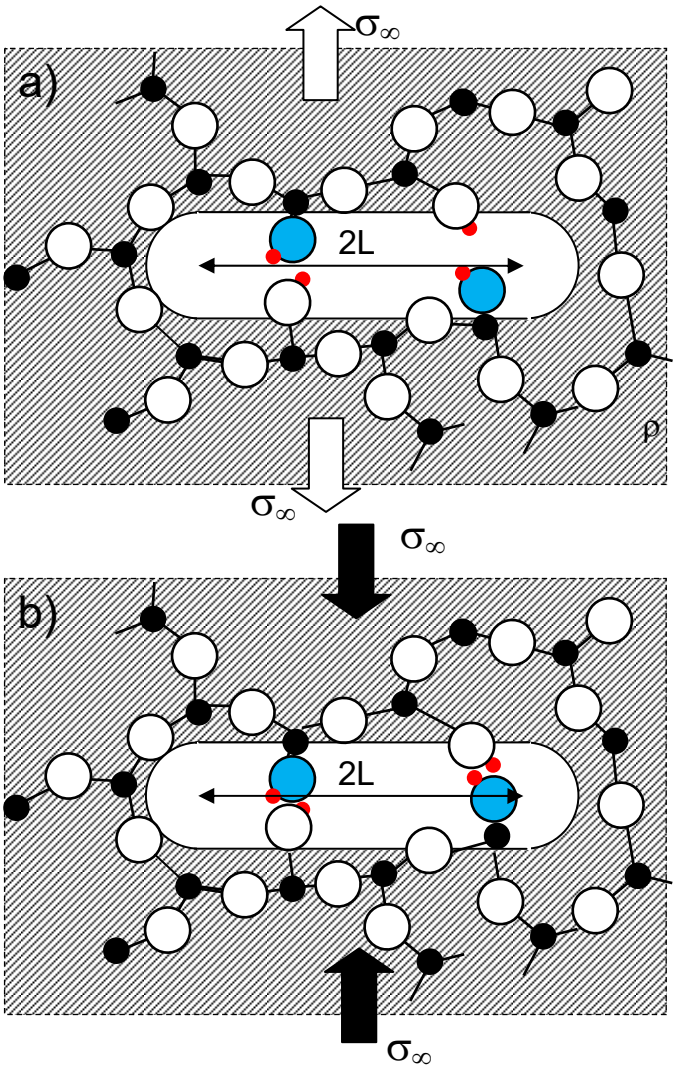

Fig. 8 a) Additionally cracked bond at a location of high stress concentration, b) limit case of a wedge-like contact of the hydroxyls under compression.

Figure 8b shows the case, when the reacted bonds are closed again by remote compressive stresses. Then it must hold $h<1$. In the ideal limit of a "hard", wedge-like contact it would be $h\rightarrow 0$ as occurs for cracks oriented normal to the stress.

The void under tensile loading acts as a disk-like defect of length $2(\rho+L)$ oriented perpendicular to the load direction. As the result of a Finite Element study, the stress increase $\sigma_{max}/\sigma_\infty$ at the notch root is shown in Fig. 9a as a function of the length L (circles).

A rough representation of these data may be given by the simple relation

$$\frac{\sigma_z}{\sigma_\infty} = 1.48 \times \sqrt{1.84 + \frac{L}{\rho}} \qquad (21)$$

The maximum displacement in the centre is given in Fig. 9b. The straight-line dependency is represented by

$$\delta_z \frac{E}{\rho\sigma_\infty} = 2 + 1.275\frac{L}{\rho} \tag{22}$$

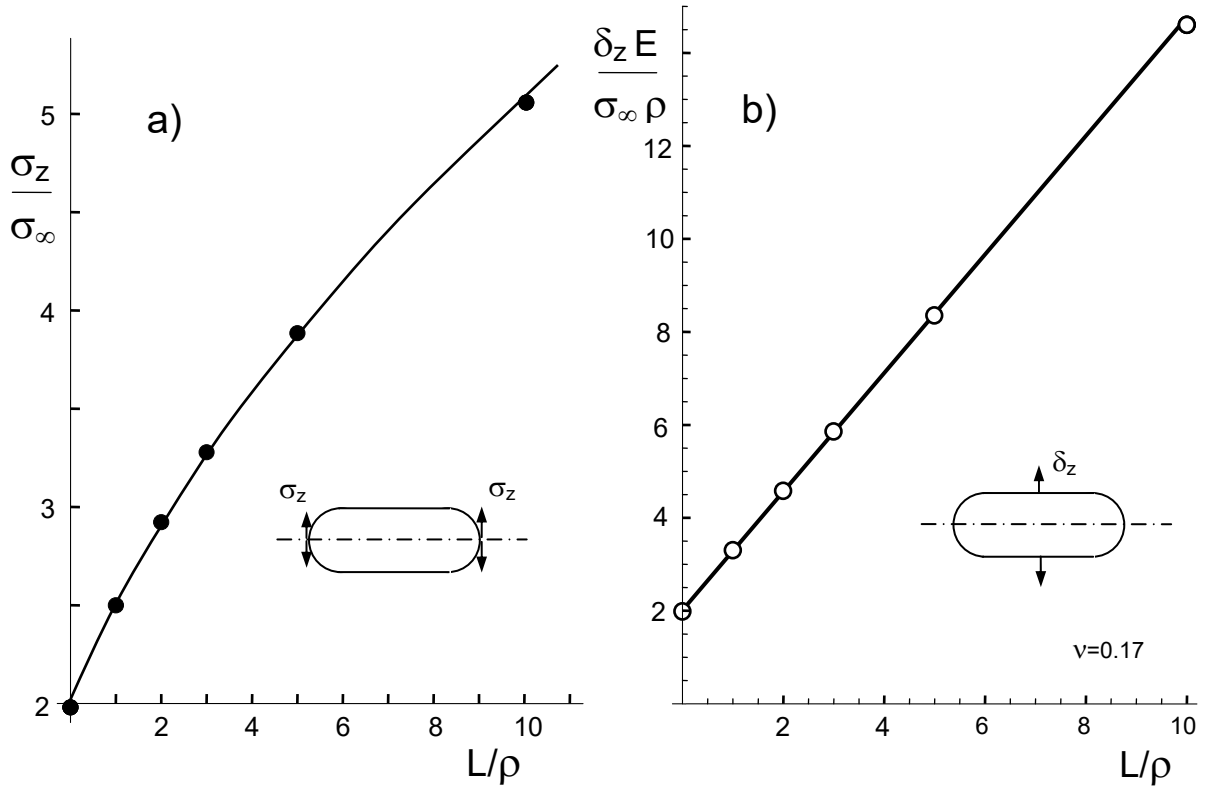

Fig. 9 a) Stress concentration at the notch root for several values of notch length *L* (circles: FE-results, curve: approximation by eq.(21), b) displacements in the axis direction, straight line: eq.(22).

References

1 H. Le Chatelier, *C.R. Acad. Sci. Paris* **99**(1884), 786.

2 F. Lechenault, D.L. Rountree, F. Cousin, J.-P Bouchaud, L. Ponson and E. Bouchaud, "Evidence of Deep Water Penetration in Silica during Stress Corrosion Fracture," Phys. Rev. Let. **106**(2011), 165504.

3 T. Fett, G. Schell, C. Bucharsky, Hydroxyl Damage in Silica: Full-range description including large damages **126**, 2019, ISSN: 2194-1629, Karlsruhe, KIT.

4 Phani, K.H. Niyogi, K. De, Young's modulus of porous brittle solids, J. Mater. Sci. **22**(1987), 257–263.

5 D. Ashkin, R.A. Haber, J.B. Wachtman, Elastic properties of porous silica derived from colloidal gels, J. Am. Ceram. Soc., 73(1990), 3376-81.

6 *Mathematica*, Wolfram Research, Champaign, USA.

7 S. M. Wiederhorn, F. Yi, D. LaVan, T. Fett, M.J. Hoffmann, Volume Expansion caused by Water Penetration into Silica Glass, J. Am. Ceram. Soc. **98** (2015), 78-87.

8 McMeeking, R.M., Evans, A.G., Mechanics of Transformation-Toughening in Brittle Materials, J. Am. Ceram. Soc. **65**(1982), 242-246.

9 J. Lemaitre, How to use damage mechanics, Nuclear Engng. Design **80**(1984), 233-245.

10 J. Lemaitre, J.P. Sermage, One damage law for different mechanisms, Comp. Mech., **20**(1997), 84-88.

11 K.G. Schell, T. Fett, C. Bucharsky, Crack-tip shielding in silica at room temperature, **135**, 2020, ISSN: 2194-1629, Karlsruhe, KIT.

12 S.M. Wiederhorn, E.R. Fuller, Jr. and R. Thomson, "Micromechanisms of crack growth in ceramics and glasses in corrosive environments," Metal Science, **14**(1980), 450-8.

KIT Scientific Working Papers
ISSN 2194-1629

www.kit.edu